Originally published 11 February 2010; corrected 26 March 2010

www.sciencemag.org/cgi/content/full/science.1186112/DC1

Supporting Online Material for

Dark Matter Search Results from the CDMS II Experiment

The CDMS II Collaboration*

*To whom correspondence should be addressed: Jodi Cooley
E-mail: cooley@physics.smu.edu

Published 11 February 2010 on *Science* Express
DOI: 10.1126/science.1186112

This PDF file includes:

SOM Text
Figs. S1 to S4
References

Correction: In the last sentence of the caption for Fig. S4, the description of the generation of the red curve was revised.

Supporting Online Material For: Dark Matter Search Results from the CDMS II Experiment

Z. Ahmed, D.S. Akerib, S. Arrenberg, C.N. Bailey, D. Balakishiyeva, L. Baudis, D.A. Bauer, P.L. Brink, T. Bruch, R. Bunker, B. Cabrera, D.O. Caldwell, J. Cooley,* P. Cushman, M. Daal, F. DeJongh, M.R. Dragowsky, L. Duong, S. Fallows, E. Figueroa-Feliciano, J. Filippini, M. Fritts, S.R. Golwala, D.R. Grant, J. Hall, R. Hennings-Yeomans, S.A. Hertel, D. Holmgren, L. Hsu, M.E. Huber, O. Kamaev, M. Kiveni, M. Kos, S.W. Leman, R. Mahapatra, V. Mandic, K.A. McCarthy, N. Mirabolfathi, D. Moore, H. Nelson, R.W. Ogburn, A. Phipps, M. Pyle, X. Qiu, E. Ramberg, W. Rau, A. Reisetter, T. Saab, B. Sadoulet, J. Sander, R.W. Schnee, D.N. Seitz, B. Serfass, K.M. Sundqvist, M. Tarka, P. Wikus, S. Yellin, J. Yoo, B.A. Young, J. Zhang

*To whom correspondence should be addressed; Jodi Cooley, E-mail: cooley@physics.smu.edu.

WIMP detector design

The 30 WIMP detectors are grouped into five "towers," each containing a stack of six detectors. Detectors are labeled by their tower number (T1-T5) and their position within that tower (Z1-Z6). Adjacent detectors in a tower face each other with no intervening material. This allows the identification of low-energy electrons via coincident scattering in neighboring detectors.

The top and bottom flat surfaces of each detector are patterned with phonon and ionization sensors, respectively. The top surface is instrumented with four phonon readout channels, each

consisting of 1036 superconducting tungsten transition-edge sensors (TESs) (*?*). Each TES is connected to Al collection fins. Out-of-equilibrium phonons from particle interactions in the crystal create quasiparticles in these fins, which in turn heat the TES. The recoil energy and position of each particle event can be reconstructed from the resulting changes in TES electrical resistance. These phonon sensors also act as the ground reference for the ionization measurement. The bottom surface is patterned into two concentric grids that function as ionization electrodes. The distorted electric field at the edge of the detector leads to poor charge collection. Events with a signal in the outer ionization readout channel are thus discarded, defining a fiducial volume. For further details of these detectors, see (*1*).

Data analysis

Summary of WIMP selection criteria

The data selection criteria (cuts) that define the WIMP acceptance region were developed using calibration sets of electron and nuclear recoils obtained during regular *in situ* exposures of the detectors to ^{133}Ba and ^{252}Cf sources. Candidate WIMP scatters were required to be within 2σ of the mean ionization yield of nuclear recoils and at least 3σ away from the mean ionization yield of electron recoils, have recoil energy between 10 and 100 keV, and have ionization energy at least 4.5σ above the noise level. They were further required to occur within the ionization fiducial volume and satisfy data quality criteria. An electron recoiling in the first few μm of the detector surface (a surface event) has ionization yield similar to that of a nuclear recoil, but has faster phonon timing. We thus require that a candidate event have phonon timing that is characteristic of a nuclear recoil. Finally, since WIMPs are expected to interact only once in the experimental apparatus, a candidate event was required to have energy deposition consistent with noise in the other 29 detectors (single-scatter event) and to have no significant activity in the surrounding scintillator shield from -185 to $+20$ μs relative to the event trigger.

Data selection

All 30 detectors were used to identify particle interactions, but only the Ge detectors were used to search for WIMP scatters. Five Ge detectors were not used for WIMP detection because of poor performance or insufficient calibration data; four more detectors were similarly excluded during subsets of the four data-taking periods. For this exposure, we did not complete the full analysis for WIMP scatters in the Si detectors due to their lower sensitivity to coherent nuclear elastic scattering; the Si detectors are used only to identify multiple-scatter events.

Periods of poor detector performance were identified and excluded from analysis on a detector-by-detector basis. Data-quality criteria were developed using Kolmogorov-Smirnov tests performed on an array of parameter distributions. Special effort was made to exclude periods of poor detector "neutralization" by monitoring the ionization yield distribution. At the low temperatures required to operate the phonon sensors, impurities and defects in the crystal detector substrate can produce isolated charge "trapping centers." Our detectors required regular neutralization of these trapping centers (*1*) to maintain full ionization collection. After applying these data quality selections, the total exposure to WIMPs considered for this work was 612 kg-days.

Calibration

The energy calibration of each detector was determined using a 356 keV γ-line from from the ^{133}Ba source. This calibration was confirmed at low energies using the 10.36 keV x-ray emission line from the electron-capture decay of ^{71}Ge, which is produced through neutron activation of our crystal substrates. Based upon the width of this line, the 1σ ionization-energy resolution at the 10 keV analysis threshold was typically ≤ 0.4 keV for the detectors considered.

Phonon pulse shapes vary with event position and energy in our detectors. To improve energy resolution and enhance surface-event rejection (see below), we characterized the observed

variation of the resulting timing and energy estimators using our electron-recoil calibrations and corrected for it in both WIMP-search and calibration data. To ensure that this correction works well at large radius, where position reconstruction degeneracies can lead to miscorrection, we included calibration electron-recoil events outside the ionization fiducial volume in the correction calculation. This technique is an improvement over that which we used on earlier data (*2*), obviating the need for an additional fiducial volume cut in phonon position reconstruction parameters. After correction, the phonon energy resolution is comparable to that of the ionization channels at low energies.

Nuclear recoil selection

Nuclear recoils from the elastic scattering of neutrons emitted by the ^{252}Cf source were used to define the ionization yield acceptance region. The acceptance region was taken to be the 2σ band about the mean neutron ionization yield (2σ nuclear recoil band) and varied as a function of recoil energy (Fig. 1). These nuclear recoils were also used to develop the surface event rejection cut and measure the signal efficiency, as described below.

Surface event rejection

The sum of the rise time of the largest phonon pulse with its delay relative to the ionization signal was empirically found to provide the best discrimination between surface events and nuclear recoils. We optimized this cut using nuclear and surface electron recoils from the ^{252}Cf and ^{133}Ba calibration exposures. Surface-event rejection criteria based on this discriminator were tuned on the calibration data by maximizing the expected sensitivity for a 60 GeV/c^2 mass WIMP. Figure 1 demonstrates our surface-event rejection capability on the calibration data.

Signal efficiency

The fractional acceptance (efficiency) of our analysis cuts for nuclear recoils was measured as a function of energy using both neutron-calibration and WIMP-search data. The fiducial volume estimate was corrected for the systematic effects of neutron multiple-scattering by using Monte Carlo simulations. Our efficiency for signal events has a maximum of 34% at 20 keV. It falls to $\sim$25% both at 10 keV, due to ionization threshold and flaring of the electron-recoil band; and at 100 keV, due to a drop in fiducial volume. After all selection criteria, the spectrum-averaged equivalent exposure for a WIMP of mass 60 GeV/c^2 is 194.1 kg-days. The efficiency at various stages of cut application is shown in Fig. 2.

Data blinding

Immediately following event reconstruction and calibration, we excluded from study all events in the entire exposure satisfying the following criteria: single-scatter events with no coincident activity in the scintillator shield and ionization yield within the 3σ nuclear band. All events in this "masked" group (which includes all potential WIMP candidate events) were automatically removed from the data files distributed to collaboration members, and so had no effect on the development of the analysis criteria. The masked events which did not meet the WIMP-selection criteria defined earlier in this work were restored to the analysis in the final stages of development for the surface-event cut and the surface event background estimate. Any candidate WIMP events remained hidden until all selection criteria were finalized and the choice of statistical technique for the limit calculation (Yellin optimum interval (*11*)) was made. On November 5, 2009, the entire data set was "unblinded": all remaining masked events were restored to analysis. Two candidate events satisfying all analysis criteria were observed in this complete data set.

Background estimates

Expected neutron background

Neutrons with energies of several MeV can generate single-scatter nuclear recoils that are indistinguishable from possible dark matter interactions. We consider two major sources of background neutron events: cosmic-ray muons interacting in or near the experimental apparatus (cosmogenic neutrons) and radioactive processes in materials making up and surrounding the apparatus (radiogenic neutrons).

The location of the Soudan Underground Laboratory, beneath a rock overburden equivalent to 2090 meters of water, greatly mitigates the background rate due to cosmogenic neutrons. Nearly all of the remaining cosmogenic neutrons are identified (vetoed) by coincident activity in the scintillator shield. Three such vetoed single-scatter nuclear recoil events were observed in this exposure, whereas none had been seen in previous CDMS II data. We used Monte Carlo simulations to estimate the remaining background from unvetoed cosmogenic neutrons. Simulations of muon-induced particle showers and subsequent neutron production were performed with Geant4 (*3, 4*) and FLUKA (*?, 6*). Good agreement was found between both simulation packages in the predicted ratio of unvetoed to vetoed neutrons, as well as in the ratio of single- to multiply-scattering neutrons, but their predictions of the absolute event rate differed. We thus took as our background estimate the product of the observed number of vetoed single-scatter nuclear recoils (three) with the ratio of unvetoed to vetoed single-scatter nuclear recoils determined from Monte Carlo. This resulted in a more conservative estimate than that produced by either package on its own. This procedure, combined with corrections for efficiency and exposure time, predicts $0.04^{+0.04}_{-0.03}$(stat) unvetoed, cosmogenically-produced, single-scatter nuclear recoils in the reported data.

Our estimate of the radiogenic neutron background due to spontaneous fission and (α, n)

processes was informed by measurements of samples of our shielding and detector materials, which were screened for U and Th daughters using high-purity Ge gamma counters. We also derived an independent estimate of the contamination levels of U and Th from a fit of the electromagnetic spectrum observed by our experiment to a Monte Carlo simulation. The combined estimate of contamination levels, together with the assumption of secular equilibrium, were used as input to a detailed Geant4 simulation that propagated the resulting neutrons through the experimental setup. The estimated radiogenic neutron background is between 0.03 and 0.06 events and is dominated by U spontaneous fission in the Cu cans of the cryostat. The radiogenic neutron background originating from the surrounding rock is estimated to be negligibly small in comparison to other sources.

Expected surface event background, prior to unblinding

The number of misidentified surface events was estimated by multiplying the observed number of single-scatter events failing the timing cut inside the 2σ nuclear-recoil band by the expected ratio of events passing the timing cut to those failing it (the "pass-fail ratio"). This ratio was estimated using a combination of three methods with differing statistical and systematic errors:

1. The first method computed the pass-fail ratio from events that reside within the 2σ nuclear-recoil band and multiply scatter in vertically adjacent detectors (multiple-scatter events).

2. The second method uses multiple-scatter events surrounding the 2σ nuclear-recoil band (wide-band events). Wide-band events have different distributions in energy and in detector face (ionization- or phonon- side) from nuclear-recoil band events, affecting the pass-fail ratio. To account for these differences, the pass-fail ratio of these events was corrected using the face and energy distributions of events observed in the nuclear-recoil band that failed the timing cut.

3. A third, independent estimate of the pass-fail ratio was made using low-yield, multiple-scatter events in ^{133}Ba calibration data, again adjusted for differences in energy and detector-face distributions.

All three estimates were consistent with each other and were thus combined to obtain an estimate prior to unblinding of 0.6 ± 0.1(stat) surface events misidentified as nuclear recoils.

Expected surface event background, after unblinding

After unblinding, a detailed study motivated by one of our candidate events revealed that an approximation made during the ionization pulse reconstruction degrades the timing-cut rejection of a small fraction of surface events with ionization energy below $\sim$6 keV. Such events are more prevalent in WIMP-search data than in the data sets used to generate the estimate of misidentified surface events prior to unblinding. A refined calculation, which accounted for this reconstruction degradation, revised the surface-event estimate to 0.8 ± 0.1(stat)± 0.2(syst) events from the prior estimate of 0.6 ± 0.1(stat). The systematic uncertainty in this final estimate is dominated by the uncertainty in our assumption that the pass-fail ratio for multiple scatter events is the same as that for single scatter events.

Discussion of results

Additional information on the unblinded data

Figure 3 shows events on all detectors after all selection criteria have been applied, except the yield and timing cuts. Candidate events appear in the signal region of detectors T1Z5 (at 12.3 keV) and T3Z4 (at 15.5 keV). The dates and local times of the two candidate events are October 27, 2007 at 14:41 CDT (T1Z5 event) and August 5, 2007 at 20:28 CDT (T3Z4 event). Both occur during periods of good experimental performance. The candidate event observed

with detector T3Z4 suffers from the ionization reconstruction effect described in the previous paragraph, which increases the possibility for it to be a surface event.

Varying the timing cut

To quantify the proximity of these events to the surface-event rejection threshold, we varied the timing cut threshold of the analysis. Reducing the revised expected surface-event background to 0.4 events would remove both candidates while reducing the WIMP exposure by 28%. No additional events would be added to the signal region until we increased the revised estimate of the expected surface-event background to 1.7 events. The corresponding limits that are obtained with these cut values are shown in Fig. 4. The figure also shows that while the allowed surface-event background chosen by the blind analysis gives, on average, the best expected limit over the range shown, the actual observed limit is never more than 15% higher in the range of 0.1 to 6 expected surface events.

Details of the inelastic scattering calculation

We computed DAMA/LIBRA regions allowed at 90% C. L. following the χ^2 goodness-of-fit technique described in (*7*). We apply quenching factors of 0.30 (Na) and 0.09 (I) (*8*) and do not include channeling effects (*9*). Limits from our data and that of XENON10 (*10*) were computed using the optimum interval method (*11*). We used an escape velocity of 544 km/s (*12*) and a constant relative scintillation efficiency of 0.19 for XENON10. Regions excluded by CDMS and XENON10 were defined by demanding the 90% C. L. upper limit to completely rule out the DAMA/LIBRA allowed cross section intervals for allowed WIMP masses and mass splittings.

References and Notes

1. D. S. Akerib, *et al.*, *Phys. Rev.* **D72**, 052009 (2005).

2. Z. Ahmed, *et al.*, *Phys. Rev. Lett.* **102**, 011301 (2009).

3. S. Agostinelli, *et al.*, *Nucl. Instrum. Meth.* **A506**, 250 (2003).

4. J. Allison, *et al.*, *IEEE Trans. Nucl. Sci.* **53**, 270 (2006).

5. A. Fasso, *et al.* (2003).

6. A. Ferrari, P. R. Sala, A. Fasso, J. Ranft (2005). CERN-2005-010.

7. C. Savage, G. Gelmini, P. Gondolo, K. Freese, *JCAP* **0904**, 010 (2009).

8. R. Bernabei, *et al.*, *Phys. Lett.* **B389**, 757 (1996).

9. R. Bernabei, *et al.*, *Eur. Phys. J.* **C53**, 205 (2008).

10. J. Angle, *et al.*, *Phys. Rev.* **D80**, 115005 (2009).

11. S. Yellin, *Phys. Rev.* **D66**, 032005 (2002).

12. M. C. Smith, *et al.*, *Mon. Not. Roy. Astron. Soc.* **379**, 755 (2007).

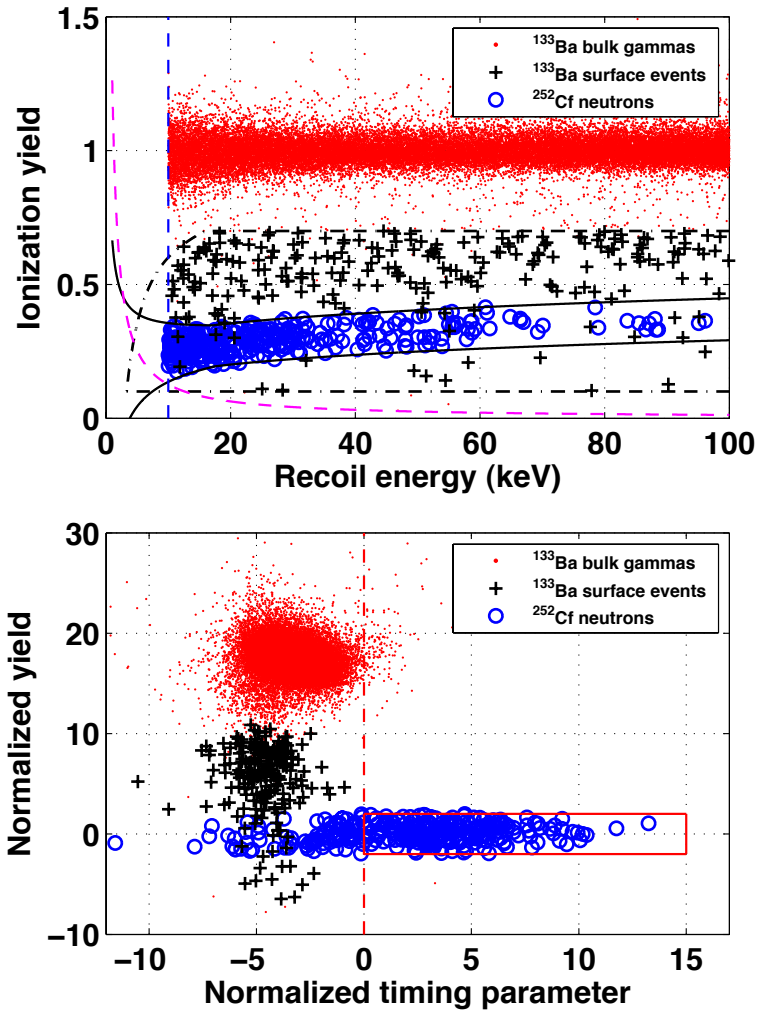

Figure S1: The power of the primary background discrimination parameters, ionization yield and phonon timing, is illustrated for a typical detector using *in situ* calibration sources. Shown are bulk electron recoils (red points), surface electron events (black crosses) and nuclear recoils (blue circles) with recoil energy between 10 and 100 keV. Top: Ionization yield versus recoil energy. The solid black lines define bands that are 2σ from the mean nuclear-recoil yield. The sloping magenta line indicates the ionization energy threshold while the vertical dashed line is the recoil energy analysis threshold. The region enclosed by the black dash–dotted lines defines the sample of events that are used to develop surface-event cuts. Bottom: Normalized ionization yield (number of standard deviations from mean of nuclear recoil band) versus normalized timing parameter (timing relative to acceptance region) is shown for the same data. Events to the right of the vertical red dashed line pass the surface-event rejection cut for this detector. The red box is the WIMP signal region.

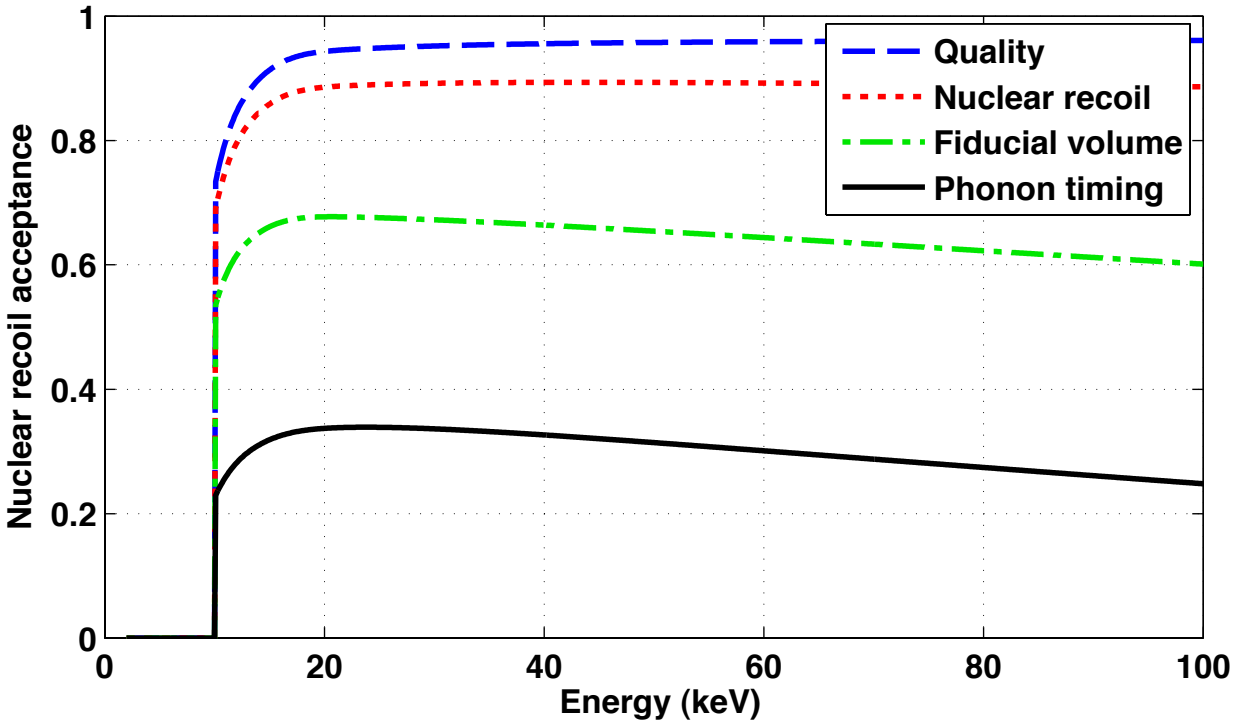

Figure S2: Cumulative efficiency as a function of recoil energy after application of each WIMP-selection cut shown. The solid curve shows the overall efficiency of this analysis. The drop in efficiency near 10 keV is due to the ionization threshold and the flaring of the electron recoil band. The slight drop in efficiency at high recoil energies is due to a drop in the fiducial volume.

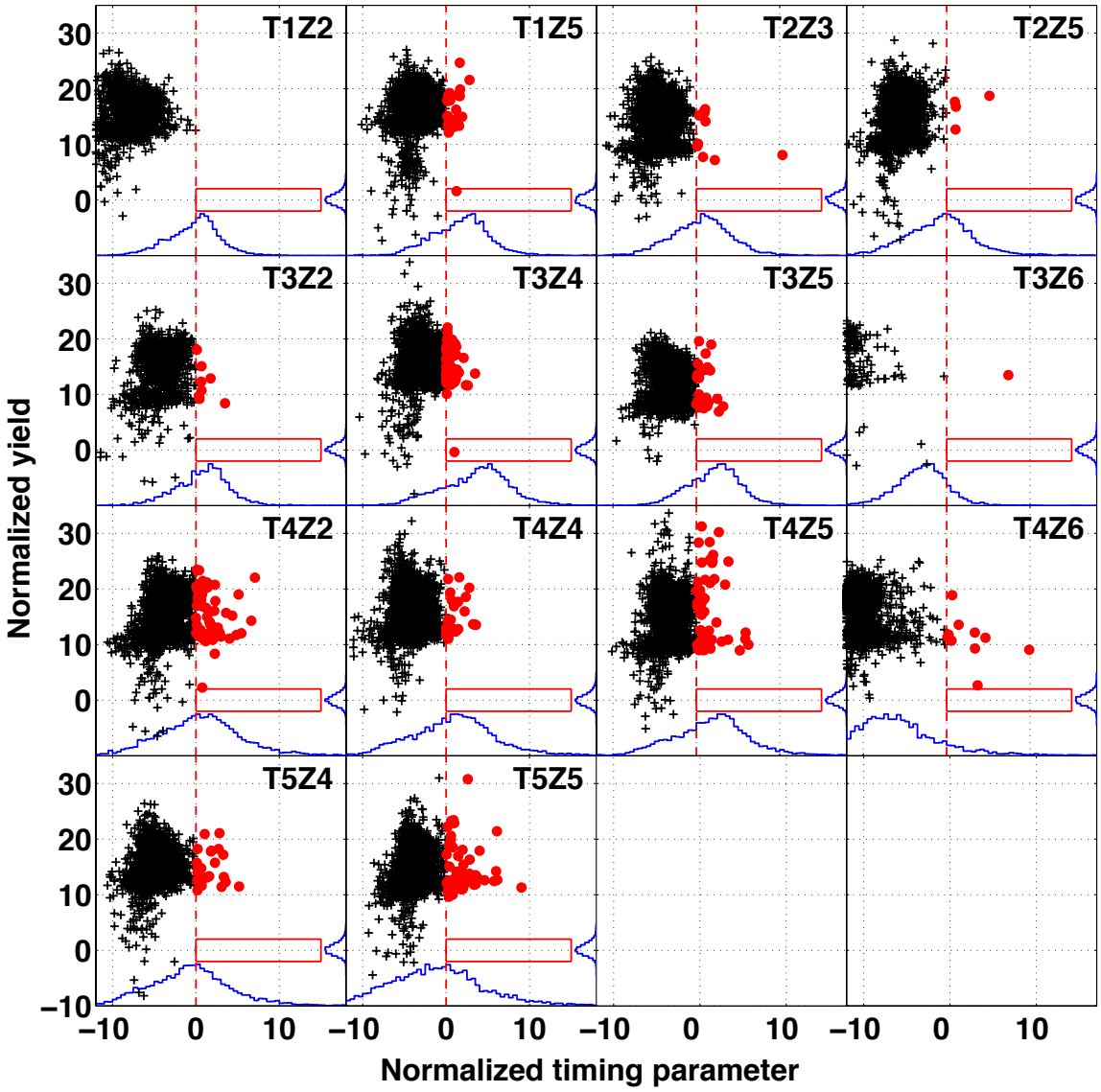

Figure S3: Normalized ionization yield (number of standard deviations from mean of nuclear recoil band) versus normalized timing parameter (timing relative to acceptance region) for all events and with all cuts applied except for yield and timing. Each panel shows the data taken with the indicated detector. Data for all detectors that were used in this reported WIMP search are shown. Events that pass the phonon timing cut are shown with round markers. The red boxes indicate the signal region for that detector. The blue histograms shows the expected distributions for nuclear recoils in each detector, as measured by the calibration data.

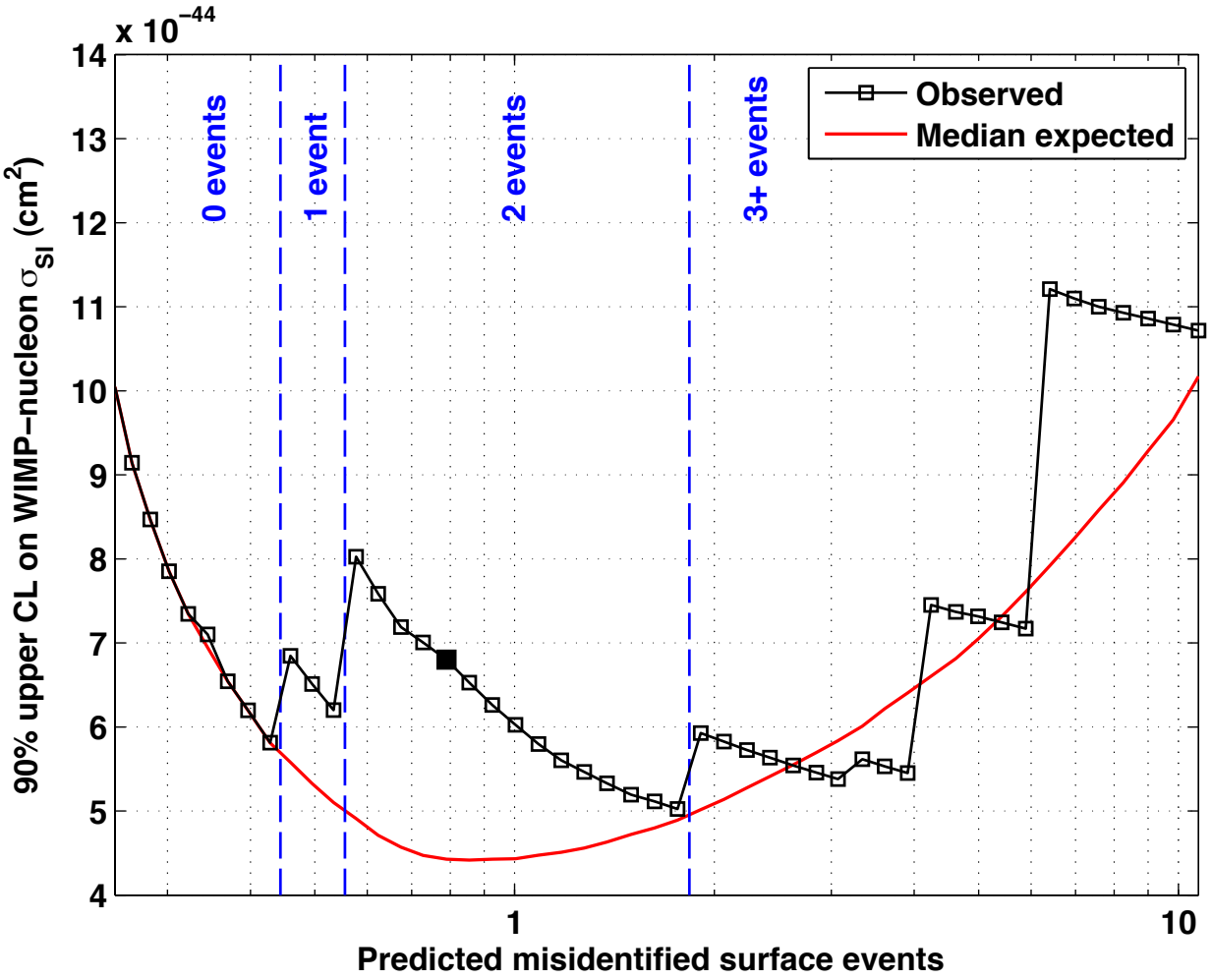

Figure S4: The observed 90% C.L. upper limit, at a WIMP mass of 70 GeV/c^2, as a function of predicted misidentified surface event background. The solid square shows the observed limit from the choice of timing cut value used in the blind analysis, which corresponds to the indicated misidentified surface event prediction. The open squares show the limits that would have been observed for other choices of timing cut value. The blue dashed lines mark the transitions at which additional background events would appear. The red curve is generated by taking the median of many limits, each of which is obtained by drawing a value from a Poisson distribution with mean value given by the corresponding value of predicted misidentified surface events.